INTERSTELLAR MOLECULAR LINES IN THE DIRECTION OF THE YOUNG STAR TY CrA

JASON A. CARDELLI[a)]
Washburn Observatory, University of Wisconsin–Madison, Madison, Wisconsin 53706

GEORGE WALLERSTEIN[a)]
Astronomy Department, University of Washington, Seattle, Washington 98195
Received 5 October 1988; revised 6 December 1988

ABSTRACT

We present echelle data ($\lambda/\Delta\lambda \approx 40\,000$) for lines of CN, CH, and CH^+ in the direction of TY CrA, a line of sight associated with a dense, young star-forming region. The line of sight resides adjacent to a dense, collapsing cloud rich in molecules. The dust in the complex appears highly processed with values of λ_{max} (the wavelength of maximum polarization) and R_v [$\equiv A_v/E(B-V)$] that are considerably larger than normal. For TY CrA, R_v could be as high as 7. The implication is that the UV extinction is probably flat (e.g., like θ Ori), with the absolute UV extinction relative to the visual, A_{UV}/A_v, being well below the average curve. The relative abundances of CN and CH may suggest relatively high densities, perhaps in excess of 10^3 cm^{-3}. However, in comparison to HD 29647 ($R = 3.6$) with similar A_v (≈ 3 mag) and perhaps density, the molecular abundances are low. Comparison to model abundances indicates that this difference can be largely explained by the differences in A_{UV}/A_v between the two lines of sight (e.g., photochemistry is much more active toward TY CrA). The CH^+ data indicate a velocity shift relative to the other lines of about $\Delta V \approx 2$ km s^{-1}. We interpret this as implying that CH^+ is formed in a weak shock that is probably associated with the local cloud collapse. Comparison to magnetohydrodynamic shock models indicates that the large abundances of CH^+ and CH are consistent with a shock with a velocity of $V_s \approx 10$ km s^{-1}, seen at an angle from the normal to the shock front of $\theta \approx 70°$, and a radiation-field-enhancement factor of $\chi \approx 3$–5. This latter parameter is consistent with the absolute UV-to-optical extinction, A_{UV}/A_v, being rather low toward TY CrA as implied by the large R_v value.

I. INTRODUCTION

A wealth of good-quality interstellar molecular absorption-line data of species like CH, CH^+, CN, C_2, and H_2 now exist in the literature. Most of these data sample diffuse interstellar clouds (i.e., $A_v < 2$ mag within the cloud) where photochemical processes are expected to dominate. As the quality and diversity of the data have increased, tighter constraints have been placed on chemical models, since any successful model must satisfy all of the observational constraints. Recent theoretical models of such environments have appeared in the literature that handle a number of observational constraints with varied success (for an excellent review of the status of models of diffuse clouds, see van Dishoeck and Black 1988). In diffuse clouds, the dominant mechanism for the destruction of neutral molecules arises through photodissociation and photoionization by ultraviolet photons. Consequently, successful models must consider the effects of attenuation of UV radiation by dust, where careful consideration should be paid to systematic variations of UV-to-optical extinction, A_{UV}/A_v (Cardelli 1988).

Expansion of the database to include semi-opaque lines of sight (i.e., $A_v > 2$ mag) sets new constraints on existing models (van Dishoeck and Black 1989, hereafter referred to as vDB). Such lines of sight begin to probe regions where photochemistry should play a relatively minor role deep in the cloud, but where the depth dependence into the cloud must still be considered (van Dishoeck and Black 1988). A further complication is that, in the more heavily reddened lines of sight, complex molecules begin to form. However, one must be cautious in assuming that all heavily reddened lines of sight fall into this category (e.g., dense, dark clouds). Heavily obscured stars observed over long path lengths sometimes sample multiple diffuse clouds or single, denser clouds for which a substantial amount of dust exists *outside of the molecular environment.*

In this paper, we present data for the line of sight to TY CrA, a young star in a very young star-forming region containing numerous T Tauri and Herbig Ae/Be stars (Knacke *et al.* 1973; Vrba, Strom, and Strom 1976; Wilking, Taylor, and Storey 1986). The spectrum of this star shows strong lines of CN, CH, and CH^+. With $E(B-V) \approx 0.46$, one might not consider this to be a heavily reddened line of sight. However, $E(B-V)$ alone is not necessarily indicative of the amount of obscuration. For a given $E(B-V)$, a line of sight with a large value of total-to-selective extinction, R_v [$\equiv A_v/E(B-V)$], has a much higher visual obscuration than a line of sight with a nominal value of $R_v = 3.1$. R_v values in the CrA cloud near TY CrA range from 3.6 to 6.0.

Of particular interest is the rather strong presence of CH^+. Understanding the production of CH^+ in clouds has long been a problem. Calculations based on chemical equilibrium in a quiescent cloud fail to predict column densities of CH^+ that match observed values. It seems likely that CH^+ is formed under special conditions, such as behind weak shocks (Elitzur and Watson 1978, 1980). Support for shock production comes from observed correlations between the abundance of CH^+ and excited levels of H_2 ($J = 3$–5: Frisch and Jura 1980; Lambert and Danks 1986). However, the shock models mentioned above fail because they tend to overproduce OH and rotationally excited H_2. Use of magnetohydrodynamic (MHD) shocks by Draine and Katz (1986a,b, hereafter referred to as DK) appear to produce acceptable amounts of OH and H_2 ($J = 3$–5). However, these models appear unable to reproduce the higher populations observed in the $J = 6,7$ levels (Draine 1986),

[a)] Visiting Astronomer, Cero Tololo Inter-American Observatory, which is managed by the Association of Universities for Research in Astronomy, Inc., for the National Science Foundation.

 0004-6256/89/041099-11$00.90

which appear to require additional photon pumping (van Dishoeck and Black 1988).

Lines of sight such as TY CrA supply important new data for a variety of reasons. First, the relatively close proximity and high galactic latitude of the cloud complex ($d \approx 130$ pc, $b \approx -18°$, Marraco and Rydgren 1981) effectively minimize foreground contamination. In addition, at our resolution ($\lambda/\Delta\lambda \approx 40\,000$), no evidence of multiple components is seen for any line, including Ca II, implying that additional components are confined to $\Delta V \leqslant 7$ km s^{-1}. If multiple components exist, they are probably localized. Finally, the relative youth of the region and the very large values of R_v indicate that this complex is well suited for examining the properties of gas and dust in a highly processed state.

Below we present the velocities and column densities for various observed species and compare them with other observations of the CrA cloud, as well as abundances observed in other clouds. In Sec. II, we describe the observations, reductions, and derivation of abundances. In Sec. III, we describe the environment and general chemistry.

II. THE DATA

a) Observations and Reductions

The observations presented here were obtained in 1984 June with the 4 m echelle spectrograph at CTIO. The detector consisted of IIIa-J photographic plates behind the long blue camera and image intensifier. The spectra have a resolution of about 50 μm on the plate, corresponding to about 0.10 Å resolution ($\lambda/\Delta\lambda \approx 40\,000$) at the dispersion of 2.1 Å mm^{-1} (at 4000 Å). Both spectra were widened to about 0.6 mm to provide maximum signal to noise within the exposure times of 126 and 206 min. Comparison spots were impressed both before and after each exposure. Radial velocities for all of the lines were measured on each plate using the Grant oscilloscope comparator at the University of Colorado, Boulder. The derived velocities appear in Table I.

The plates were traced using the University of Washington microdensitometer and were converted to intensity via tracings of calibration plates obtained during the observing run. This was done for each order of interest as well as the interorder background on either side. For each order, the adjacent backgrounds were fit with a smooth function, averaged, and then subtracted.

Table II contains the measured line data and abundances. Column (1) lists the molecular/atomic species, column (2) lists the applicable transition, column (3) lists the laboratory wavelengths, column (4) lists the oscillator strengths (f values), column (5) lists the measured equivalent widths, and column (6) lists the derived column densities. The measured line uncertainties were derived from the line integration via a propagation of errors using the noise in the neighboring continuum and assuming that this noise is constant throughout the line. These uncertainties also included a continuum fitting "error," added in quadrature to the line uncertainty, adopted to be $\pm$ 50% of continuum noise about the best-fit continuum. The curve of growth analysis and associated errors are discussed below. The f values are those used by Cardelli and Wallerstein (1986) and are essentially the same (within a few percent) as those adopted by Black and van Dishoeck (1988). The wavelengths for CH lines were taken from Black and van Dishoeck (1988). For CH^+ λ 3957 and λ 4232, the wavelengths were taken from Hawkins, Jura, and Meyer (1985), which were derived from the Carrington and Ramsey (1982) vacuum wavelengths.

A final note concerns the reliability of photographic data. It is true that photographic data suffer from numerous uncorrectable problems including limited dynamic range, nonuniformities, nonlinearities, and fixed pattern noise (i.e., in the case of image tubes). However, carefully exposed and reduced photographic data, while inherently noisier, can yield reliable measurements for well-detected lines (e.g., the photoelectric results of Danks, Federman, and Lambert (1984) and Lambert and Danks (1986) compared with the photographic results of Chaffee (1975)). Any gross systematic errors are more likely the result of careless reduction, which can affect solid-state detector data as well.

b) Derivation of Abundances

Because the data show effects of saturation, the derivation of abundances requires use of the curve of growth which requires a knowledge of the turbulent velocity b. If we assume that the level population of CN is controlled by excita-

TABLE I. Radial-velocity data.

	Heliocentric Velocity (km s^{-1})[a]						
	Interstellar[b]				Stellar		
Plate	CH^+	CH	CN	Ca II	Ca II	Fe II	Si II
1749	-5.3	-4.3	-3.4	-3.6	+74.2	+68.3	+73.9
1756	-5.3	-2.9	-2.7	-3.3	-75.0	-77.5	-76.2

[a]The conversion to LSR velocity is +7.4 km s^{-1}

[b]The mean velocity error is about 0.7 km s^{-1}

TABLE II. Observed data.

Species	Transition			λ(Å)	f[a]	W_λ (mÅ)[b]	Log N[c]
CN	$B^2\Sigma^+ - X^2\Sigma^+$	(0,0)	R(0)	3874.61	0.0342	21	
			R(1)	3874.00	0.0228	13	
			P(1)	3875.76	0.0114	8[d]	13.45[e]
CH	$A^2\Delta - X^2\Pi$	(0,0)	$(T_{2e}+T_{2f})$	4300.31	0.0053	28	
	$B^2\Sigma^- - X^2\Pi$	(0,0)	(T_{2f})	3886.41	0.0032	10[d]	
			(T_{2e})	3890.22	0.0021	8[d]	13.70[f]
CH^+	$A^1\Pi - X^1\Sigma^+$	(0,0)	R(0)	4232.55	0.0056	28	
		(1,0)	R(0)	3957.69	0.0034	17	13.70
Ca II K				3933.68	0.688	27	11.45[g]
Ca I				4226.73	1.61	≤ 6	≤ 10.4

[a]Oscillator strengths: taken from Cardelli and Wallerstein (1986) and references therein.

[b]Equivalent width uncertainies ≈ 2.5-3 mÅ except where noted.

[c]Logarithm of the derived column densities (in cm^{-2}). In the case of CN, log N refers to the total abundance (i.e. $N_0 + N_1$).

[d]These lines are poorly detected with uncertainties of about ±4-5 mÅ.

[e]Log N derived assuming $b_{CN} \approx 0.6$ km s^{-1} which corresponds to $T_{exc} = 2.76$ K (see text).

[f]Log N derived using $b_{CH} \approx 1.0$ km s^{-1} which follows from b_{CN} (see text).

[g]Derived from linear curve-of-growth (see text). For b ≈ 1.0 km s^{-1}, log N = 11.7.

tion from the microwave background ($T_{exc} = 2.76$ K, Meyer and Jura 1985; Crane *et al.* 1986), we find $b_{CN} \approx 0.6$ km $s^{-1} \pm 0.3$ km s^{-1}. (Possible problems with this assumption are discussed in the Appendix.) The limits on b were estimated by applying the uncertainty of the $R(0)$ and $R(1)$ measurements in opposing directions. From this approach, the larger b value yields log $N(CN) \approx 13.2$, while the smaller value yields log $N(CN) \approx 13.6$. In the region around the denser part of the cloud, the radio data of Loren (1979), excluding CO, yields an average line full width at half maximum of $\langle \Delta V \rangle \approx 1.3$ km s^{-1} with a range of about ± 0.5. From 6 cm H_2CO absorption measurements, Dieter (1975) found $\Delta V = 0.7$ km s^{-1} toward TY CrA ($\Delta V = 1.2$ km s^{-1} toward R and T CrA). If we assume that this value represents an upper limit (the optical data sample a much smaller solid angle and possibly a smaller line-forming region), then $b = \Delta V/2(\ln 2)^{1/2} \leqslant 0.4$ km s^{-1} (for $\Delta V = 1.2$ km s^{-1}, $b \leqslant 0.7$ km s^{-1}). These limits are consistent with the value found from assuming excitation by the microwave background and implying that $b < 1$ km s^{-1}.

For CH, the λ 4300 line is an unresolved blend of two lines, separated by $\Delta V = 1.43$ km s^{-1}, arising from a Λ doublet ($J = 1/2$) state (see Table II). Consequently, the value of b_{CH} will be larger than the "true" turbulent velocity b (see Lien 1984; Cardelli and Wallerstein 1986). Adopting $b \approx b_{CN} = 0.6$ km s^{-1} and the discussion of Lien (1984), we find $b_{CH} \approx 1.0$ km s^{-1}. We have assumed that $N(T_{2e}) = N(T_{2f})$, which is consistent with the measured limits for λ 3886 and λ 3890. If we assume that $b \approx 1$ km s^{-1} (similar to the upper limit in b for CN) we find $b_{CH} \approx 1.5$ km s^{-1}, which results in a decrease in log N(CH) given in Table II of about 0.10. Conversely, a value of b similar to the lower limit found for CN results in an increase in log N(CH) of about 0.12. (For comparison of the abundances of CH and CN,

one should be aware these associated error estimates are coupled through the adopted b value.)

For the two lines of CH^+, the best fit to the curve of growth is found for $b \approx 1.1$ km s^{-1} (a value as high as 1.4 km s^{-1} results in essentially the same abundance) with an uncertainty in the log of the abundance of about ± 0.10. Since the velocity shift relative to the other lines implies that it is formed in a different region, possibly behind a shock, it is not surprising that the CH^+ lines could not be fitted to the same curve of growth as CN and CH.

We were only able to observe the K line of Ca II and so we cannot independently derive b. The value listed in Table II was derived using the linear part of the curve of growth (the result is essentially the same for $b \geqslant 5$ km s^{-1}). Because Ca II might be expected to exist in a much larger portion of the cloud than the molecules, a larger b value would not be unexpected. For $b \approx 1$ km s^{-1}, the abundance increases by about 0.25 in the log.

III. DISCUSSION

a) The Corona Australis Dark Cloud

1) The general environment

TY CrA resides within the R CrA dark cloud, a region of very recent star formation rich in molecular gas and dust. As stated above, this region is extremely well suited for study since the effects of foreground contamination are minimized. A map of the CrA region is shown in Fig. 1. The contours in the figure show the general distribution of gas and dust in the complex. The dark and dashed lines represent the visible dust boundaries within which the cloud appears opaque. The H I contours (Vaile and Taylor 1982) show a "hole" in the atomic hydrogen distribution centered about 20′ southeast of R CrA, which has been interpreted as a region of possible cloud collapse (Llewellyn *et al.* 1981) and where the gas is presumably largely H_2.

The light squares in Fig. 1 represent the locations where the peak antenna temperature (T_A) of OH reaches a maximum (Vaile and Taylor 1982) with the contours of constant T_A running in a southeast–northwest direction. The long-dash contour in Fig. 1 represents the maximum extent of the 6 cm H_2CO absorption observed by Vaile and Taylor 1982, which also follows this southeast–northwest line. Similar spatial distribution is also seen for 2 mm and 2 cm lines of H_2CO (Nachman 1979; Gross *et al.* 1980; Loren, Sandqvist, and Wootten 1983) although the observations do not extend as far to the southeast as the 6 cm data. Other molecules observed in this region include CO (Loren 1979; Nachman 1979; Vaile and Taylor 1982), CS (Turner *et al.* 1973; Loren 1979), SO, HCN, and HCO^+ (Loren 1979).

A major concentration of molecular gas appears to coincide with the region around R CrA (Morris *et al.* 1974; Loren 1979), northwest of the H I hole. However, Loren (1979) also finds a peak in T_A ($^{12,13}CO$) toward TY CrA and concludes that this star is a dominant heating source in the cloud. The presence of these molecules suggests that the region located at and around R CrA is rather high in density and is probably collapsing (Loren 1979). From an analysis of their H_2CO data, Loren, Sandqvist, and Wooten (1983) find that the density is highest toward the position of R CrA ($n > 4 \times 10^5$ cm^{-3}) with the contours of constant density again following a southeast–northwest line. At the position of TY CrA, the inferred density is $n \approx 3 \times 10^4$ cm^{-3}. Evidence of star formation in this region includes a number of embedded 2 μm sources (Glass and Penston 1975; Vrba, Strom, and Strom 1976) including a small infrared cluster (Taylor and Storey 1984; Wilking, Taylor, and Storey 1986). Brown and Zuckerman (1975) found evidence for two compact H II regions suggesting the presence of some embedded early-type stars.

Evidence of recent star formation ($< 10^6$ yr; Knacke *et al.* 1973) outside the dense core also exists. Most of the visible

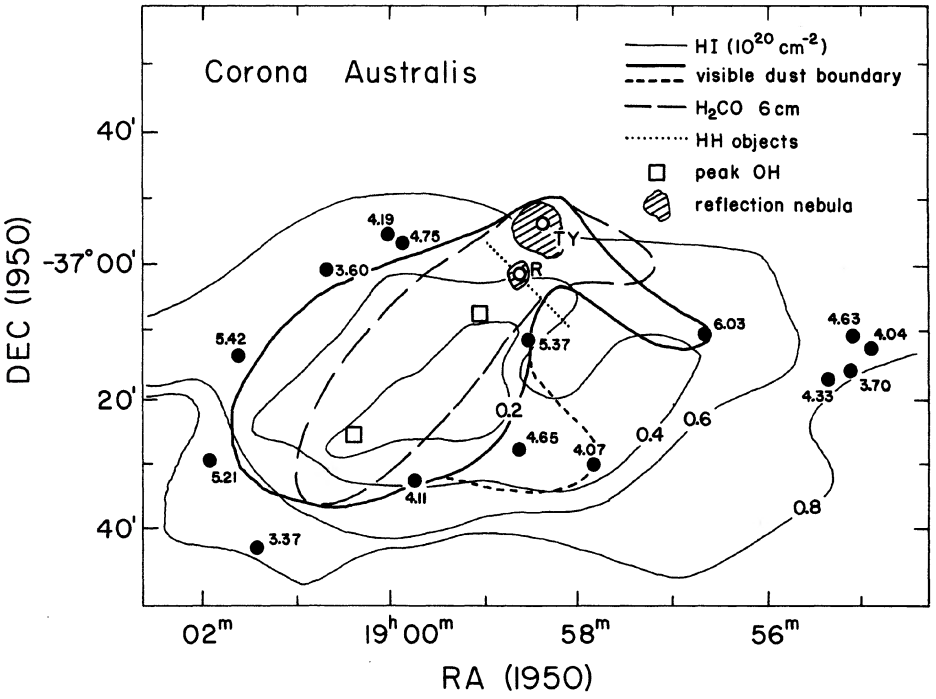

FIG. 1. Map of the Corona Australis cloud region. The positions of TY and R CrA are marked. The light squares represent the positions where the observed peak antenna temperature of OH reaches a maximum. The long-dash line outlines the maximum spatial extent of 6 cm H_2CO observed by Vaile and Taylor (1982). The dotted line shows the direction and extent of the distribution of HH objects. The dark circles represent stars in the complex. The numbers indicate the value of R_v [$\equiv A_v / E(B-V)$] for each star.

stars are later than type A (Vrba, Coyne, and Tapia 1981; Vrba and Rydgren 1984) and many are also associated with near-IR excesses (Knacke *et al.* 1973; Vrba, Strom, and Strom 1976; Wilking, Taylor, and Storey 1986). A number of these objects are also Herbig Ae/Be and T Tauri stars (Herbig and Rao 1972; Marraco and Rydgren 1981). Other indications of relative youth include a number of HH objects (Strom, Strom, and Grasdalen 1974; Vrba, Strom, and Strom 1976; Schwartz, Jones, and Sirk 1984). The dotted line running through the position of R CrA in Fig. 1 gives the direction and spatial extent of these objects (Hartigan and Graham 1987).

Observations of interstellar dust in the CrA cloud also exhibit evidence characteristic of young star-forming regions. Vrba, Coyne, and Tapia (1981) mapped the polarization in the cloud and found that λ_{max}, the wavelength of maximum polarization, ranges between 0.45 and 1.1 μm and has a mean value of nearly 0.8 μm. Such large values of λ_{max} imply larger than normal grains, which in the case of CrA may be as much as a factor of 2 (Vrba, Coyne, and Tapia 1981). Other evidence of larger grains comes from values of the ratio of total-to-selective extinction, $R_v \equiv A_v / E(B-V)$, measured toward a number of stars in the CrA region (Vrba and Rydgren 1984). Values of R_v for a number of stars are shown in Fig. 1. These values show a clear systematic increase toward the more opaque portion of the cloud. The interpretation of these results is consistent with that implied by the polarization data which indicate that the grains in the CrA cloud are significantly larger than normal. As with other regions with large R_v values (e.g., the ρ Oph cloud), significant grain growth in CrA is associated with regions of large gas densities through processes that probably include coagulation. In the CrA cloud, the lack of massive young stars and their associated strong radiation fields has undoubtedly helped promote grain growth. In the denser portion of the cloud, the possibility also exists for the depletion of molecules like H_2CO onto grains (Loren, Evans, and Knapp 1979; Vrba, Coyne, and Tapia 1981).

2) TY CrA

The spectral classification of TY CrA is B9 (Herbig and Rao 1972; Knacke *et al.* 1973; Glass and Penston 1975). Comparison of the stellar lines present in our data to similar observations of other B stars (Cardelli and Wallerstein 1986) indicates that TY CrA is most likely type B8–B9.

As indicated in Fig. 1, TY CrA is associated with the reflection nebula NGC 6726/7. Based on mid-IR photometry, Wilking, Taylor, and Storey (1986) conclude that TY and R CrA are the dominant luminosity sources near the embedded core. This conclusion was also reached by Knacke *et al.* (1973). The nature of the IR spectrum seen towards TY CrA (Wilking, Taylor, and Storey 1986) indicates that the dust in this direction is relatively cool ($T_d \leqslant 100$ K). This suggests that this star is either immediately behind the edge of the main distribution of material or has evacuated a cavity surrounding the star.

From the published optical/near-IR data of Knacke *et al.* (1973) and Vrba, Strom, and Strom (1976), we derived a value for R_v toward TY CrA using the techniques outlined in Clayton and Mathis (1988) and Cardelli, Clayton, and Mathis (1988,1989, hereafter referred to as CCM). Assuming an uncertainty in the spectral type, we find $R_v \approx 7.0$ (B7; $E(B-V) = 0.52$), 7.4 (B9; $E(B-V) = 0.46$), and 8.3 (A0; $E(B-V) = 0.42$). (The analysis of Wilking, Taylor, and Storey (1986) also indicates a very large R_v value with even larger values being indicated for R and T CrA). Noting the distribution of larger-than-normal R_v values for this cloud (see Fig. 1), these values are not inconsistent. The fact that they are much larger than those for the other lines of sight may indicate that the grain processing is even more extensive toward the dense core. However, because TY CrA as well as R and T CrA are associated with rather bright reflection nebulosity, contamination from scattering by dust into the entrance aperture can result in lower extinction toward the blue relative to the near-IR, resulting in an overestimate of R_v. For example, Schiffer and Mathis (1974) found that, for the Orion Nebula, the flux of scattered light increases by about a factor of 3 between $\lambda \approx 7000$ and 5500 Å (the V bandpass) and a factor of 5 between $\lambda \approx 7000$ and 4400 Å (the B bandpass). We unfortunately do not have any information on the relative contribution of scattering toward TY CrA. However, if we use an analogy to systems of similar physical characteristics and reddening (e.g., NGC 7023/HD 200775—Witt *et al.* 1982; NGC 1999/V380 Ori—Warren-Smith 1983), we find that accounting for the effects of nebular contamination results in an increase of $E(B-V)$ of 0.03–0.06 mag. For the B9 comparison, we find that these changes in $E(B-V)$ decrease R_v from 7.4 to 6.9 and 6.5, respectively. While R_v is considerably reduced, these values still indicate that R_v is much larger than normal, consistent with the other values found in the complex.

b) Kinematics

The heliocentric velocities for the observed species are shown in Table I. The uncertainty in these values is of the order of 0.7 km s^{-1}. The LSR velocities of the CH and CN lines are 1.5–2.0 km s^{-1} smaller than those observed for the radio lines. This difference could imply that our data arise in an absorbing region in front of the cloud giving rise to the radio lines. However, Cardelli and Wallerstein (1986) found an identical discrepancy between their LSR velocities for HD 147889 and those derived from radio data and the optical data of Crutcher and Chu (1985). Cardelli and Wallerstein (1986) attributed this difference to probable systematic errors in their data (no velocity standards were observed). Since the data presented here were obtained on the same observing run as the Cardelli and Wallerstein data, the LSR velocity difference for TY CrA is probably also systematic. We therefore feel that velocities of CN and CH are in reasonable agreement with the radio results.

c) General Chemistry: Comparison to Existing Data

1) The effects of variable extinction on the abundance of CN and CH

The CN and CH abundances for TY CrA are plotted in Fig. 2 along with data taken from Crutcher (1985, HD 29647), Jannuzi *et al.* (1988, HD 169454), and Cardelli, Suntzeff, and Savage (1988, HD 62542). These points have been included for comparison because they also show CN column densities in excess of 10^{13} cm^{-2} and because $N(CN)/N(CH)$ is of the order of 1. The solid lines in Fig. 2 are taken from the model analysis of Federman and Lambert (1988) and represent high ($n = 2500$ cm^{-3}, $T = 25$ K) and low ($n = 150$ cm^{-3}, $T = 50$ K) density limits. Also shown are the model results of vDB (Table 10, the first row for models T2–T5) which correspond to $n \approx 500$–1000 cm^{-2}, $T \approx 15$–40 K, and values of $A_v = 1.3$, 2.0, 3.0, and 3.9 mag. The general association of the data points with these model

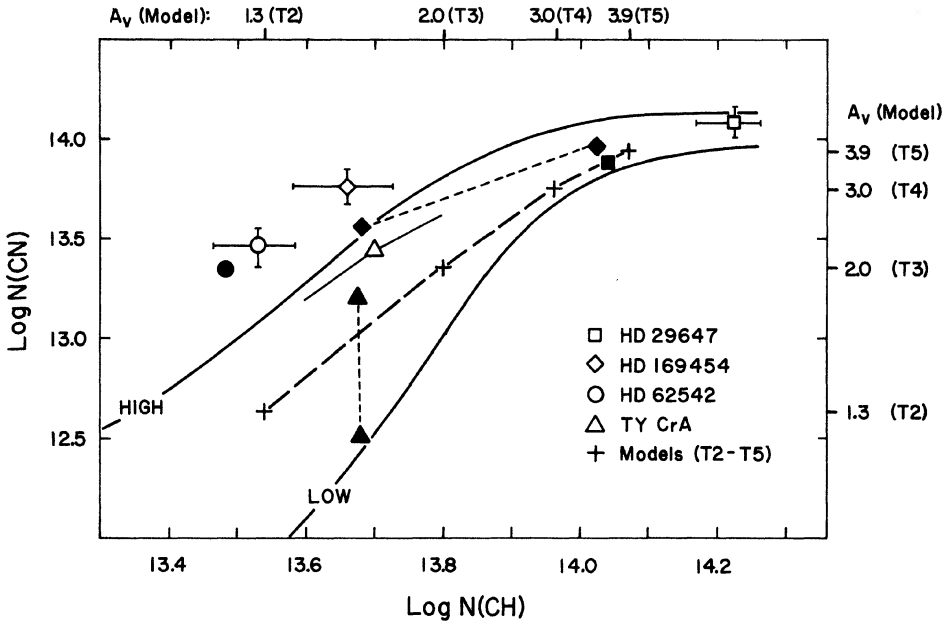

FIG. 2. Logarithm of the abundance of CN versus CH for TY CrA along with data taken from the literature (see text). The lines associated with the data point for TY CrA correspond to the b value coupled uncertainties. The solid lines represent the model results of Federman and Lambert (1988) corresponding to high ($n = 2500$ cm^{-3}, $T = 25$ K) and low ($n = 150$ cm^{-3}, $T = 50$ K) density limits. The plus symbols, connected by a long dash, correspond to models T2–T5 of vDB (the corresponding model and input A_v are indicated along the axes). The dark symbols correspond to model estimates for the four stars, found by comparing the observed values of A_{UV} with those applicable to the models (see Table III) over the wavelengths corresponding to photodestruction of CH and CN.

density limits would seem to characterize these lines of sight as tending toward higher density material. However, exactly where a particular point resides depends upon a complex combination of important factors including density, depletion of carbon, nitrogen, and oxygen, adopted unattenuated radiation field, and the absolute UV extinction. With the exception of extinction, these other factors are difficult to measure directly for a particular line of sight. Consequently, we pose the following question. If we assign the same physical parameters (e.g., density, depletion, and unattenuated radiation field; models T2–T5 of vDB) to all four lines of sight, to what degree will the position of a particular data point depend upon the wavelength dependence of the absolute extinction?

The adopted absolute extinction data A_λ for these stars are shown in Table III for $\lambda = 3000, 2000, 1500$, and 1000 Å. These wavelengths were chosen because they represent the ranges where primary photodestruction of CH (1500 Å$\leqslant\lambda\leqslant$3000 Å) and CN ($\lambda\leqslant$1000 Å) occur. Also shown are the corresponding A_λ values derived from the average curve of Seaton (1979) for four values of A_v used in the models of vDB. With the exception of TY CrA, A_{3000}, A_{2000}, and A_{1500} were derived from published UV extinction curves (HD 169454—Seab, Snow, and Joseph 1981; Savage *et al.* 1985, HD 29647—Snow and Seab 1980; Cardelli and Savage 1988, HD 62542—Cardelli and Savage 1988) through the adopted values of the total-to-selective extinction, R_v [$\equiv A_v/E(B-V)$], shown in the table. These R_v values we derived directly for HD 29647 and TY CrA from optical/near-IR extinction data. For HD 169454 and HD 62542, no near-IR data are available. However, from the analysis of CCM it can be shown that the $E(B-V)$ normalized extinction curves for these stars are consistent with $R_v \approx 3$ (and possibly lower for HD 62542). For TY CrA, we estimated the UV extinction by using the A_λ/A_v vs R_v^{-1} dependence from CCM. Finally, the values for A_{1000} were found by extrapolating the functional form of the far-UV curvature between 1700 and 1200 Å down to 1000 Å (see Fitzpatrick and Massa 1986, 1988, CCM) and should be considered as crude estimates only.

For TY CrA, the A_{1000} value in the parentheses corresponds to what would be expected if the curvature in the extinction curve shortward of 1500 Å were similar to that of HD 147889. For HD 169454, the values in parentheses correspond to the expected extinction to the cloud if about half of the observed $E(B-V)$ arises from *normal* (e.g., Seaton 1979) extinction between the cloud and the star. These values are included for the following reason. Jannuzi *et al.* (1988) adopt $d_c \approx 125$ pc (Crutcher and Lien 1984) to the cloud and $d_* \approx 1660$ pc to the star ($b \approx -1°$). From Crutcher and Lien (1984), $E(B-V)$ ranges from about 0 to 0.5 mag for stars in the general direction to HD 169454 characterized by 125 pc$\leqslant d_* \leqslant$300 pc. The value inferred from the Galactic plane average of 0.6 $E(B-V)$/kpc is $E(B-V) \approx 1$ mag. It is therefore possible that at least half the observed extinction is behind the cloud.

The four sets of A_λ values for the average curve given in Table III should represent the *extinctions* from which corresponding *attenuations* used in the vDB model calculations were derived (e.g., via the albedo and phase function defined by model 2 of Roberge *et al.* (1981)). We assume that the same albedo and phase function also apply to the extinction

TABLE III. Selected absolute extinction data.[a]

Object	E(B-V)	R_V	A_V	A_{3000}[b]	A_{2000}[b]	A_{1500}[b]	A_{1000}[c]
HD 29647	1.03	3.6	3.7	6.7	9.1	9.8	18.5
HD 169454[d]	1.14 (0.57)	3.0[e]	3.4 (1.6)	6.2 (3.0)	9.5 (4.1)	9.7 (4.8)	20.4 (12.0)
HD 62542	0.34	3.0[e]	1.0	1.8	2.9	3.5	10.0
TY CrA	0.48	6.5	3.1	4.0[f]	4.8[f]	4.0[f]	5.8[f] (9.3)[f,g]
Average[h]	0.42	3.1	1.3[i]	2.3	3.8	3.5	6.4
Average[h]	0.65	3.1	2.0[i]	3.6	5.8	5.4	9.8
Average[h]	0.97	3.1	3.0[i]	5.4	8.7	8.1	14.7
Average[h]	1.26	3.1	3.9[i]	7.0	11.3	10.5	19.1

[a]Absolute extinction, A_λ. The subscripts refer to wavelengths (e.g. 2000 ≡ 2000 Å, etc.).

[b]Primary wavelengths where CH photodestruction occurs.

[c]Photodestruction of CN occurs for $\lambda \leq 1000$ Å. The extinction at 1000 Å was estimated by extrapolating the function which represents the far-UV curvature (see the text).

[d]The extinction data were taken from the ANS extinction data of Savage et al. (1985). The values in parenthesis correspond to the assumption that half the extinction arises from behind the cloud (see text).

[e]See text.

[f]The extinction is derived from the A_λ/A_V vs R_V^{-1} relationship of Cardelli, Clayton, and Mathis (1988).

[g]A_{1000} using the functional form of the curvature for HD 147889 for $\lambda < 1500$ Å.

[h]A_λ calculated from the average curve of Seaton (1979).

[i]The values of A_V were chosen to correspond to models T2-T5 of van Dishoeck and Black (1989).

data for the four stars. Thus, for each star, a model CH and CN abundance can be crudely estimated by comparing the observed A_λ *for the appropriate wavelength* with the A_λ data for the average curve applicable to the models. These estimates are shown as dark symbols in Fig. 2. For HD 169454, the point representing the smaller abundances corresponds to the assumption that half of the extinction arises behind the cloud. Similarly, for TY CrA, the point representing the larger CN abundance corresponds to the assumption of a steeper far-UV extinction below 1500 Å (e.g., a functional form similar to HD 147889).

It is quite clear from the figure that, in comparison to the average curve, differences between A_λ at 1000 Å and 1500–3000 Å for the observed extinction can result in considerable displacement of the model points. The general agreement between the distribution of the model values and the actual data is quite remarkable. In reality, density, temperature, depletion, and perhaps the unattenuated radiation field appropriate for the individual lines of sight may differ considerably. For example, a lower depletion of carbon is maybe more appropriate for HD 29647. However, the purpose of our comparison was to examine how effective the variations in the shape of absolute extinction curves from the average curve are in determining the abundances and not to exactly reproduce the observed data. To this end, Fig. 2 indicates that variations in the shape of UV extinction are very important.

2) Shock formation of CH^+

The data shown in Table I indicate that the velocity of CH^+ differs from that of the other lines by about 2 km s^{-1}.

Velocity shifts of 1–2 km s^{-1} between CH and CH$^+$ have been used to support the shock formation of CH$^+$ (Federman 1982). However, when the improved CH$^+$ wavelengths (Carrington and Ramsey 1982) are used, only about half of the lines of sight show velocity shifts in excess of 1 km s^{-1} (Federman 1987). Thus, identification of additional lines of sight with velocity shifts larger than 1 km s^{-1} is useful (van Dishoeck and Black 1988a). We take the observed velocity shift toward TY CrA to indicate that the formation of CH$^+$ occurs behind a shock in this environment. However, conventional shock models (Elitzur and Watson 1980) seem unable to reproduce a CH$^+$ abundance as large as that observed toward TY CrA. The CrA region shows evidence of an ordered magnetic field that appears to be strongest in and around the major distribution of dust seen in Fig. 1, with a field strength perhaps as high as 150 μG (Vrba, Coyne, and Tapia 1981). Consequently, we shall qualitatively compare the data for TY CrA to the MHD shocks of DK. Shocks in this region can be seen to possibly arise from one of two scenarios: infall into the dense cloud toward R CrA and infall/outflow from the environment around TY CrA.

From models of DK, the observed abundance of CH$^+$ implies a shock velocity of the order 10 km s$^{-1} < V_s < 15$ km s^{-1}. If we assign the average velocity of all of the other lines to the preshock gas, then this range of V_s corresponds to a velocity shift between these lines and CH$^+$ of 7 km s$^{-1} < \Delta V < 12$ km s^{-1} in the direction perpendicular to the shock front. This shift is reduced to what is observed if θ, the angle between the line of sight and the normal to the shock front, is about 73°–80°. If we adopt $\theta \approx 73°$, from DK we find that the observed column density of CH$^+$ is reproduced for $V_s \approx 10$ km s^{-1} with $\Delta V \approx 2$ km s^{-1}. The above result requires that χ, the radiation-field-enhancement factor, is about 3. The factor χ is usually considered in terms of an increase in the unattenuated radiation. However, it can also be viewed in terms of a decrease in A_{UV}/A_v relative to the adopted model values. Consequently, $\chi > 1$ seems reasonable for the TY CrA line of sight considering the probable low value of A_{UV}/A_v, which follows from the large value of R_v (CCM). It is also of interest to note that the computed line-of-sight velocity dispersion σ for CH$^+$, which results from a combination of the kinematic and thermal dispersions computed by DK, is consistent with the turbulent velocity found from the curve of growth fit. Finally, the implied geometry is, in principle, consistent with a shock originating on the surface of the infalling cloud toward R CrA but does not seem consistent with infall/outflow around TY CrA.

There are some potential problems with the above simplified analysis. The DK model indicates that shock conditions like those above will also produce a significant amount of CH in the postshock region, specifically $N(CH^+) \approx N(CH)$, with $V(CH^+) - V(CH) \approx 1$ km s^{-1}. Realistically, both preshock and postshock components probably exist. Unfortunately, we are unable to make any direct statements concerning the possible existence of such closely spaced ($\Delta V < 2$ km s^{-1}) components (b could not be directly computed from the CH data). However, for the conditions specified above and assuming equal contribution from preshock and postshock CH, the computed shift between CH$^+$ and the *combined* (unresolved) CH components is about 1.5 km s^{-1}. This could be made larger by decreasing θ or increasing the shock velocity slightly, although this value is within the errors of the velocity data shown in Table I. Also, while a shift between this *mean* CH velocity and that of the preshock gas of the order 0.5 km s^{-1} is expected from the above arguments, we cannot reliably determine from our data that one exists. If two components do exist, then one can expect an increase in the curve of growth turbulent velocity for CH relative to the gas in the preshock region (e.g., CN). As discussed in Sec. II*b* above, a larger b for CH is certainly possible. For equal components, the total abundance of CH is reproduced by requiring that $\chi = 5$, which again is consistent with the probable low UV-to-optical extinction. Another potential problem exists in that the models of DK use

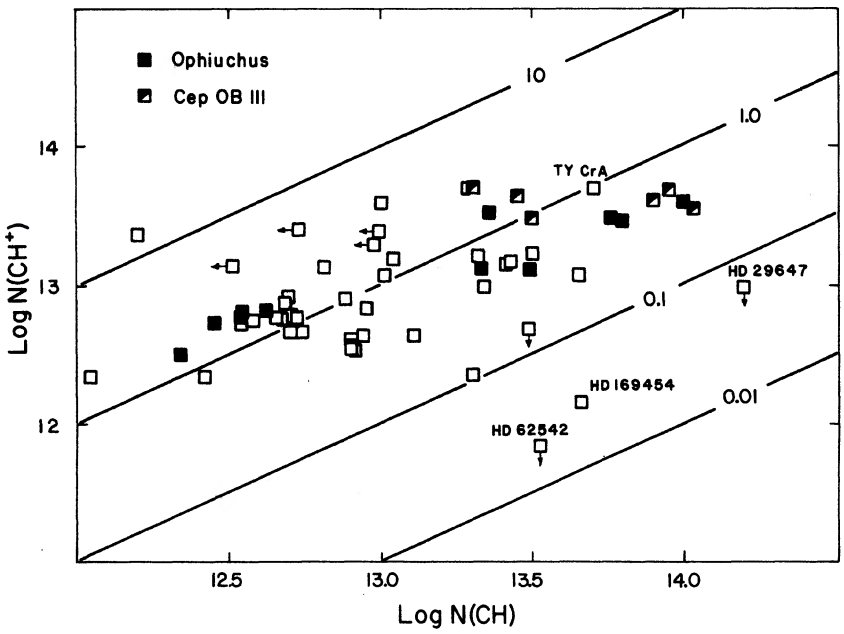

FIG. 3. The logarithm of the abundance CH$^+$ versus CH for TY CrA along with data from the literature. The abundances for two associations have also been indicated (the Cep OB III data are from Cardelli and Smith 1988). The solid lines represent different constant ratios of $N(CH^+)/N(CH)$. Note that the vast majority of the data reside between $10 \geqslant N(CH^+)/N(CH) \geqslant 0.1$. For the lines of sight to HD 29647 and HD 62542, the CH$^+$ abundances are upper limits. These lines of sight, like HD 169454, may put limits on the equilibrium abundance of CH$^+$ in cold clouds.

$n(H) \approx 50$ cm^{-3} for the preshock density. Considering the discussion of CH vs CN above, it is not clear how much of the observed abundance of CN and CH toward TY CrA can be attributed to such a preshock condition. Also, we cannot make any direct statements concerning the existence of additional unresolved components, which makes this kind of analysis difficult (see Black and van Dishoeck 1988). In any case, if the general nature of such a comparison is acceptable, then the essential results $V_s \approx 10$ km s^{-1}, $\theta \approx 70°$, and $\chi > 1$ could be considered reasonable in that they are consistent with the available information.

Figure 3 shows the relationship between CH^+ and CH for TY CrA along with other data taken from the literature. It is of interest to note that for the three lines of sight discussed in the previous subsection, $N(CH^+)/N(CH) < 0.1$ and could be as low as 0.01 for HD 29647 and HD 62542. As can be seen in Fig. 3, with one exception, all other lines of sight fall between $10 \geqslant N(CH^+)/N(CH) \geqslant 0.1$ (the models of DK cover $3 \geqslant N(CH^+)/N(CH) \geqslant 0.03$). Lines of sight where $N(CH^+)/N(CH)$ is near or even less than 0.01 may provide important limits on the equilibrium gas-phase formation of CH^+. This is particularly interesting because it was primarily the failure of the equilibrium chemistry to produce suitable CH^+ that led to the development of the theory of shock formation.

IV. SUMMARY

The data presented here represent a line of sight with significant abundances of CN, CH, and CH^+ and supplies additional data for semi-opaque environments where the density may exceed 10^3 cm^{-3}. The environment is useful to study because it represents a region of recent star formation where the dust appears to be highly processed. The ratio of total-to-selective extinction R_v is generally large for the CrA cloud and could be as large as $R = 6.5$–7 for TY CrA.

Compared to HD 29647 ($R_v = 3.6$), a line of sight with a similar A_v (≈ 3 mag) and possibly similar density, the abundances of CN and CH observed toward TY CrA are considerably reduced. Although no UV extinction data is available for TY CrA, the analysis of CCM implies that the ratio of UV-to-optical extinction A_{UV}/A_v appropriate for this line of sight is probably much lower than for HD 29647. By comparison to the models of vDB, the differences in abundances between these two lines of sight are consistent with photodestruction playing a much more active role in the chemistry toward TY CrA.

Our data give $\log N(CH^+) \approx 13.7$ with $N(CH^+)/N(CH) \approx 1$ and a velocity separation between CH^+ and the other lines of $\Delta V \approx 2$ km s^{-1}. Application of the MHD shock model of Draine and Katz (1986a,b) indicates that the observed abundances of CH^+ and CH are consistent with a shock with a velocity of $V_s \approx 10$ km s^{-1}, observed at an angle from the normal to the shock front of $\theta \approx 70°$, and a radiation field enhancement factor of $\chi \approx 3$–5. This enhancement is consistent with a low ratio of UV-to-optical extinction A_{UV}/A_v implied by the large observed R value. This result is also consistent with the assumption that the observed CH line arises from the combination of (unresolved) preshock and postshock components.

We gratefully acknowledge the many useful comments and suggestions on this manuscript given by J. H. Black, J. S. Mathis, and B. D. Savage. We also would like to thank an anonymous referee for useful criticism that resulted in some positive changes in the discussion.

APPENDIX

a) Excitation Temperature versus Abundance for CN

The turbulent velocity b for CN was derived by assuming that the population of the $N = 0,1$ levels is controlled by the

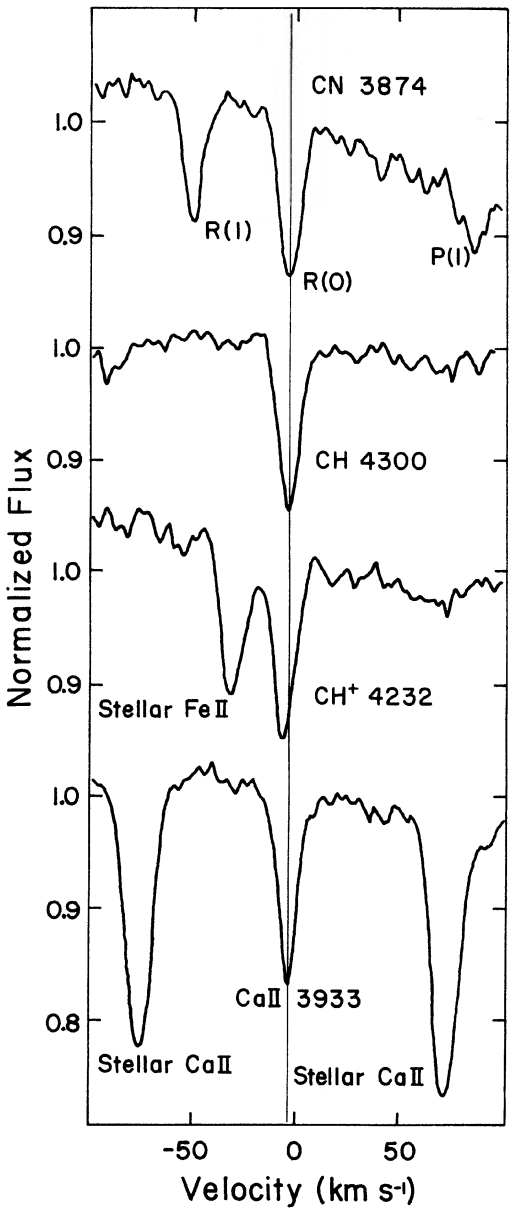

FIG. 4. Line data observed toward TY CrA plotted against heliocentric velocity. For CN, the velocity refers to the $R(0)$ line. Two stellar lines arising in TY CrA are indicated. The stellar Ca II line exhibited a velocity shift of $\Delta V \approx 150$ km s^{-1} over a 24 hr interval and consequently appears as two separate lines. A similar shift was observed for all the other stellar lines, including Fe II, the second "component" of which is shifted off the plot to the right.

microwave background. While this appears to be generally true for diffuse lines of sight (e.g. $A_v \leqslant 1$ mag: Meyer and Jura 1985; Crane *et al.* 1986), additional excitation for lines of sight with high density ($n \geqslant 10^3$ cm^{-3}) is possible (Thaddeus 1972). Indeed, millimeter-wavelength observations of hyperfine transitions of CN do indicate that additional excitation does occur (Churchwell and Bieging 1982; Crutcher, Churchwell, and Ziurys 1984). For our CN data, the saturation is large enough that the level ratio N_0/N_1 is quite sensitive to small changes in b. For example, if we assume that $b = 1$ km s^{-1}, we find $T_{exc} \approx 4$ K (since b is constrained by ΔV from the H_2CO lines, this is probably an upper limit) with log $N(CN) \approx 13.2$. Because excitation temperatures as large as this are possible, one cannot necessarily discount this result. Thus, for lines of sight with strong CN lines, *significant errors in the abundance might result from an incorrect assumption of* T_{exc}. (This problem will also apply if only the $R(0)$ line is used to derive the abundance.) A possible solution to fixing b and deriving T_{exc} would be to observe the CN (1,0) $R(0)$ line at 3579.99 Å along with the three lines near 3875 Å. Utilizing just such an approach for HD 29647, a heavily reddened star in the Taurus Molecular Cloud, Crutcher (1985) was able to establish a unique curve of growth fit with $b = 1.4$ km s^{-1}, which yields $T_{exc} \approx 2.9$ K, in reasonable agreement with what is found from the radio data. Considering that this appears to be a dense, quiescent line of sight (see Crutcher (1985) and Fig. 3), perhaps serious collisional excitation of CN only occurs for densities well in excess of 10^3 cm^{-3}, implying that our assumption of $T_{exc} \approx 2.76$ K is reasonably valid.

b) The Stellar Spectrum of TY CrA

The underlying spectrum of TY CrA is unusual. Sharp lines of Ca II, Si II, Fe II, and Mg II are present. The data shown in Fig. 4 indicates that the Ca II stellar line shifted by about $\Delta V \approx 150$ km s^{-1} over a 24 hr period. Similar shifts are also seen for other stellar lines (see Table II), including the hydrogen lines. Kardopolov, Sahanionok, and Philipjev (1981) claim that TY CrA is a short-period ($p = 2.89$ days) eclipsing binary. The observed velocity shifts are at least consistent with a short-period binary. However, binaries with periods less than about 10 days usually have their rotations phase locked to their orbital periods and consequently show rotationally broadened lines. As is evident in Fig. 4, the two stellar lines shown are quite narrow, indicating that the rotational broadening of TY CrA is surely $\leqslant 10$ km s^{-1}. In addition, from three plates taken in 1946, Herbig and Rao (1972) found a mean stellar velocity of -30 ± 4 km s^{-1} with no hint of variability and thus discount TY CrA as an eclipsing variable.

The stellar spectrum of TY CrA will have to be monitored very carefully to be understood.

Note added in proof: It has been pointed out by S. R. Federman that most or all of the CH and CN could exist in a cold, isothermal postshock component. Appreciable amounts of CH in the preshock region may suggest relatively high density, which could limit the production of CH^+. Assigning most of the CH and CN to a cold postshock component does not appreciably change the derived shock parameters but would help resolve the problem of the adopted low preshock density in the models of DK.

REFERENCES

Black, J. H., and van Dishoeck, E. F. (1988). Astrophys. J. **331**, 986.
Brown, R. L., and Zuckerman, B. (1975). Astrophys. J. Lett. **202**, L125.
Cardelli, J. A. (1988). Astrophys. J. **335**, 177.
Cardelli, J. A., Clayton, G. C., and Mathis, J. S. (1988). Astrophys. J. Lett. **329**, L33 (CCM).
Cardelli, J. A., Clayton, G. C., and Mathis, J. S. (1989). Astrophys. J. (submitted).
Cardelli, J. A., and Savage, B. D. (1988). Astrophys. J. **325**, 864.
Cardelli, J. A., and Smith, V. V. (1988). Bull. Amer. Astron. Soc. **19**, 1091.
Cardelli, J. A. Suntzeff, N. B., and Savage, B. D. (1988). In preparation.
Cardelli, J. A., and Wallerstein, G. (1986). Astrophys. J. **302**, 492.
Carrington, A., and Ramsay, D. A. (1982). Phys. Scr. **25**, 272.
Chaffee, F. H. (1975). Astrophys. J. **199**, 379.
Churchwell, E., and Bieging, J. H. (1982). Astrophys. J. **258**, 515.
Clayton, G. C., and Mathis, J. S. (1988). Astrophys. J. **327**, 911.
Crane, P., Hegyi, D. J., Mandolesi, N., and Danks, A. C. (1986). Astrophys. J. **309**, 822.
Crutcher, R. M. (1985). Astrophys. J. **288**, 604.
Crutcher, R. M., and Chu, Y. H. (1985). Astrophys. J. **290**, 251.
Crutcher, R. M., and Lien, D. J. (1984). In *The Local Interstellar Medium*, IAU Colloquium No. 81, edited by Y. Kondo, F. C. Bruhweiler, and B. D. Savage, NASA CP-2345, p. 117.
Crutcher, R. M., Churchwell, E., and Ziurys, L. M. (1984). Astrophys. J. **283**, 668.
Danks, A. C., Federman, S. R., and Lambert, D. L. (1984). Astron. Astrophys. **130**, 62.
Danks, A. C., and Lambert, D. L. (1983). Astron. Astrophys. **124**, 188.
Dieter, N. H. (1975). Astrophys. J. **199**, 289.
Draine, B. T. (1986). Astrophys. J. **310**, 408.
Draine, B. T., and Katz, N. (1986a). Astrophys. J. **306**, 655 (DK).
Draine, B. T., and Katz, N. (1986b). Astrophys. J. **310**, 392 (DK).
Elitzur, M., and Watson, W. D. (1978). Astrophys. J. Lett. **222**, L141.
Elitzur, M., and Watson, W. D. (1980). Astrophys. J. **236**, 172.
Federman, S. R. (1982). Astrophys. J. **257**, 125.
Federman, S. R. (1987). In *Astrochemistry*, IAU Symposium No. 120, edited by M. S. Vardya and S. P. Tarafdar (Reidel, Dordrecht).
Federman, S. R., and Lambert, D. L. (1988). Astrophys. J. **328**, 777.
Fitzpatrick, E. L., and Massa, D. (1986). Astrophys. J. **307**, 286.
Fitzpatrick, E. L., and Massa, D. (1988). Astrophys. J. **328**, 734.
Frisch, P. C., and Jura, M. (1980). Astrophys. J. **242**, 560.
Glass, I. S., and Penston, M. V. (1975). Mon. Not. R. Astron. Soc. **172**, 227.
Goss, W. M., Manchester, R. N., Brooks, J. W., Sinclair, M. W., Manefield, G. A., and Danziger, I. J. (1980). Mon. Not. R. Astron. Soc. **191**, 533.
Hartigan, P., and Graham, J. A. (1987). Astron. J. **93**, 913.
Hawkins, I., Jura, M., and Meyer, D. M. (1985). Astrophys. J. Lett. **294**, L131.
Herbig, G. H., and Rao, N. K. (1972). Astrophys. J. **174**, 401.
Jannuzi, B. T., Black, J. H., Lada, C. J., and van Dishoeck, E. F. (1988). Astrophys. J. **332**, 995.
Kardopolov, V. I., Sahanionok, V. V., and Philipjev, G. K. (1981). Var. Stars **21**, 589.
Knacke, R. F., Strom, K. M., Strom, S. E., Young, E., and Kunkel, W. (1973). Astrophys. J. **179**, 847.
Lambert, D. L., and Danks, A. C. (1986). Astrophys. J. **303**, 401.
Lien, D. J. (1984). Astrophys. J. **284**, 578.
Llewellyn, R., Payne, P., Sakellis, S., and Taylor, K. N. R. (1981). Mon. Not. R. Astron. Soc. **196**, 29P.
Loren, R. B. (1979). Astrophys. J. **227**, 832.
Loren, R. B., Evans, N. J., and Knapp, G. R. (1979). Astrophys. J. **234**, 932.
Loren, R. B., Sandqvist, Aa., and Wootten, A. (1983). Astrophys. J. **270**, 620.

Marraco, H. G., and Rydgren, A. E. (1981). Astron. J. **86**, 62.
Meyer, D. M., and Jura, M. (1985). Astrophys. J. **297**, 119.
Morris, M., Palmer, P., Turner, B. E., and Zuckerman, B. (1974). Astrophys. J. **191**, 349.
Nachman, P. (1979). Astrophys. J. Suppl. **39**, 103.
Roberge, W. G., Dalgarno, A., and Flannery, B. P. (1981). Astrophys. J. **243**, 817.
Savage, B. D., Massa, D., Meade, M., and Wesselius, P. R. (1985). Astrophys. J. Suppl. **59**, 397.
Schiffer, F. H., and Mathis, J. S. (1974). Astrophys. J. **194**, 597.
Schwartz, R. D., Jones, B. F., and Sirk, M. (1984). Astron. J. **89**, 1735.
Seab, C. G., Snow, T. P., and Joseph, C. L. (1981). Astrophys. J. **246**, 788.
Seaton, M. J. (1979). Mon. Not. R. Astron. Soc. **187**, 73P.
Snow, T. P. (1983). Astrophys. J. Lett. **269**, L57.
Snow, T. P., and Seab, C. G. (1980). Astrophys. J. Lett. **242**, L83.
Strom, K. M., Strom, S. E., and Grasdalen, G. L. (1974). Astrophys. J. **187**, 83.
Taylor, K. N. R., and Storey, J. W. V. (1984). Mon. Not. R. Astron. Soc. **209**, 5P.
Thaddeus, P. (1972). Annu. Rev. Astron. Astrophys. **10**, 305.
Turner, B. E., Zuckerman, B., Palmer, P., and Morris, M. (1973). Astrophys. J. **186**, 123.
Vaile, R. A., and Taylor, K. N. R. (1982). Proc. Astron. Soc. Aust. **4**, 443.
van Dishoeck, E. F., and Black, J. H. (1988). In *Rate Coefficients in Astrophysics*, edited by T. J. Millar and D. A. Wiliams (Kluwer, Dordrecht).
van Dishoeck, E. F., and Black, J. H. (1989). Astrophys. J. (in press) (vDB).
Vrba, F. J., Coyne, G. V., and Tapia, S. (1981). Astrophys. J. **243**, 489.
Vrba, F. J., and Rydgren, A. E. (1984). Astrophys. J. **283**, 123.
Vrba, F. J., Strom, S. E., and Strom, K. M. (1976). Astron. J. **81**, 317.
Warren-Smith, R. F. (1983). Mon. Not. R. Astron. Soc. **205**, 349.
Wilking, B. A., Taylor, K. N. R., and Storey, J. W. V. (1986). Astron. J. **92**, 103.
Witt, A. N., Walker, G. A. H., Bohlin, R. C., and Stecher, T. P. (1982). Astrophys. J. **261**, 492.